ACS APPLIED ELECTRONIC MATERIALS

pubs.acs.org/acsaelm Article

High-Photoresponsivity Transistors Based on Small-Molecule Organic Semiconductors

Zafrullah Jagoo,* Zachary A. Lamport, Oana D. Jurchescu, and Laurie E. McNeil

Cite This: ACS Appl. Electron. Mater. 2022, 4, 5799−5808 Read Online

ACCESS | Metrics & More | Article Recommendations | Supporting Information

ABSTRACT: We investigate the viability of 2,8-difluoro-5,11-bis(triethylsilylethynyl)anthradithiophene (diF-TES ADT) as a photosensor and show that there is a direct correlation between the absorption spectrum of the material and the magnitude of the resulting drain current in a field-effect transistor device made from it. We show that the diF-TES ADT device exhibits very high photosensitivity and photoresponsivity for green and blue light. We also propose a hybrid device structure that leverages the high absorptivities of two organic semiconductors to make a sandwich device with high phototransistor metrics across all wavelengths of visible light.

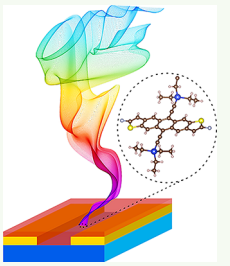

KEYWORDS: *diF-TES ADT, photocurrent, photosensitivity, photoresponsivity, photovoltaic effects, photoconductive effects*

1. INTRODUCTION

Studies on organic phototransistors to date have focused on the photodetection capabilities of thin-film transistors and rightly so, since at specific wavelengths, the performance of organic phototransistors can exceed that of silicon photodetectors.[1,2] When tunable optical/electrical characteristics are combined with the ease of processing, organic photodetectors are viable candidates for high-performance sensing and low light detection on flexible or transparent substrates. The highest photoresponse at all wavelengths of the visible spectrum that can be achieved from photocarrier generation through efficient electromagnetic absorption has been an ongoing goal to develop efficient photosensors.

2,8-Difluoro-5,11-bis(triethylsilylethynyl)anthradithiophene (diF-TES ADT) is a functionalized derivative of anthradithiophene that has been extensively studied for its high charge transport, excellent air stability, solution processability, and even bioelectric applications.[3−5] The two bulky side groups stabilize the molecule and improve solubility, and high-performance organic transistors based on this material have been demonstrated.[6] The highest reported carrier mobility of diF-TES ADT polycrystalline thin-film transistors is 20 $cm^2/(V s)$,[7] on par with that of single-crystal organic transistors and far better than amorphous silicon transistors.[8−10] In addition, diF-TES ADT has sharp absorption peaks in the visible spectrum, an attribute that we will exploit.[11] Although diF-TES ADT has superior electrical performance and can be deposited from solution, its photodetection capabilities have not been well documented.

The photoresponsivities for more than 50 organic semiconductors (polymers, polymer blends, and small molecules) have been comprehensively reviewed by Baeg et al.; however, only a few reports have tackled the photoresponsive behavior of diF-TES ADT.[12] Kim et al. illuminated a diF-TES ADT/SiO_2 transistor with white light and showed that the phototransistor had a responsivity larger than 100 mA/W at low-light intensity during device operation.[13] On the contrary, 2,8-difluoro-6,13-bis(triisopropylsilylethynyl)-anthradithiophene (diF-TIPS ADT), a material which is very similar in molecular structure and crystal packing, had not exhibited a detectable photoresponse in the visible range.[14] Higher photosensitivities and photoresponsivities imply better light detection and a more sensitive photodetector.

A more systematic study of diF-TES ADT transistors is required to see how the photoresponse is determined by the intrinsic optical characteristics of the material. In this report, we will explore the interaction of light of the three primary colors at various illumination intensities on the electrical properties of diF-TES ADT and correlate that to the absorption spectrocopy data. We found that diF-TES ADT responds exceedingly well to incident light across the visible spectrum with the highest photosensitivity with green, followed by blue, and the lowest with red illumination.

2. PHOTOCURRENT MEASUREMENTS

2.1. Experimental Details. Bottom-gate, bottom-contact organic field-effect transistors (OFETs) were fabricated on highly n-doped silicon wafers with thermally grown SiO_2, which were also the gate electrode and dielectric, respectively. These substrates were cleaned

Received: July 25, 2022
Accepted: October 31, 2022
Published: December 1, 2022

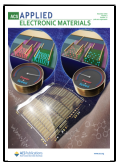

https://doi.org/10.1021/acsaelm.2c00970
ACS Appl. Electron. Mater. 2022, 4, 5799−5808

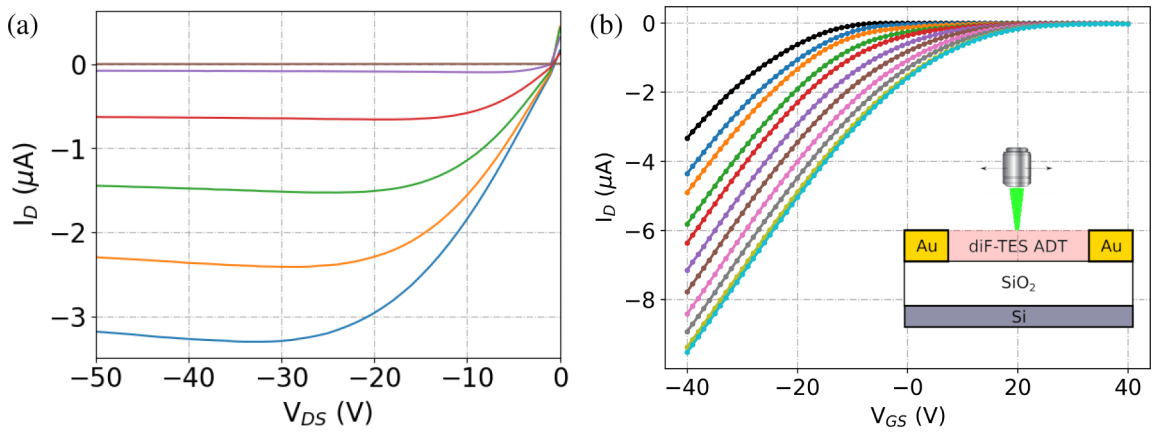

Figure 1. (a) Output characteristics of a diF-TES ADT OFET in the dark from V_{GS} = 0 to −50 V in decrements of 10 V while sweeping V_{DS}. (b) Dark (black points) and illuminated transfer characteristics of a diF-TES ADT OFET at V_{DS} = −40 V with illumination power ranging from 1.38 to 59.4 μW (colored points). The inset shows the device architecture with top transistor illumination.

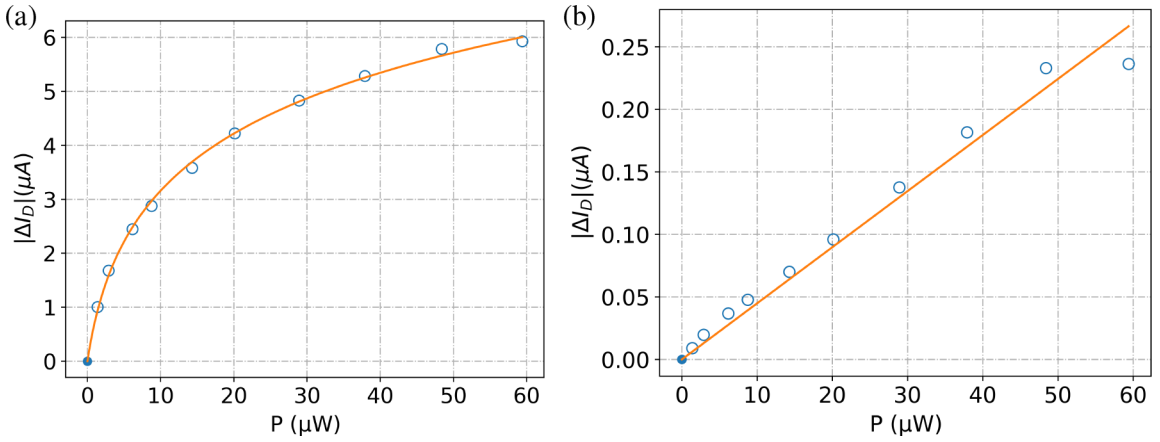

Figure 2. Photocurrent as a function of laser power when V_{DS} = V_{GS} = −40 V for the photovoltaic effect (a) and V_{DS} = −40 V and V_{GS} = +5 V for the photoconductive effect (b). The orange curves are fit to eqs 3 (a) and 5 (b) in the text.

by immersion in a bath of heated acetone (85 °C), rinsing with fresh acetone and isopropanol (IPA), and another immersion in a bath of heated IPA (85 °C). Following a subsequent rinse with fresh IPA, the wafers were dried in a stream of nitrogen and subjected to a UV/ozone treatment for 10 min, rinsed with deionized water, and dried in a stream of nitrogen. Electrodes were then evaporated through electroformed nickel shadow masks, first at 5 nm of Ti at 1 Å/s and then at 40 nm of Au at 0.5 Å/s. Immediately after electrode deposition, the electrodes were treated with a pentafluorobenzenethiol (PFBT) self-assembled monolayer (SAM) to reduce the contact resistance and enhance the morphology of the organic semiconductor. The substrates were immersed in 5 mL of ethanol with 20 μL of PFBT for 30 min and rinsed with fresh ethanol and then IPA before drying in a stream of nitrogen. The semiconductor diF-TES ADT was dissolved in chlorobenzene at a concentration of 0.5 wt % and spin coated at 1000 rpm with an acceleration of 100 rpm/s for 60 s in a nitrogen glovebox and stored overnight in a vacuum desiccator to remove residual solvent. The operational behavior of the OFETs was first verified by measuring the output characteristics (Figure 1a) in the dark by sweeping the drain−source voltage with the gate−source voltage held constant. By sweeping the gate−source voltage (V_{GS}) with the drain−source voltage (V_{DS}) held at a constant value of −40 V and measuring the drain current (I_D), the transfer characteristics, shown in Figure 1b (black points) were obtained in the dark, which were used to calculate the transistor metrics. The hole mobility in the saturation regime and the threshold voltage were calculated to be 0.03 ± 0.01 $cm^2/(V\ s)$ and −8.1 ± 0.4 V using the standard OFET analysis.[15] The linear mobility was found to be less than the saturation mobility (0.02 ± 0.01 $cm^2/(V\ s)$) due to the voltage drop arising from the contributions of the contact resistance.[16,17] The bottom-gate bottom-contact device architecture is shown in the inset of Figure 1b. The device under investigation had a channel length (L) and width (W) of 50 and 800 μm, respectively.

Light was then focused from a 532 nm (green) laser source to a spot centered between the source and drain electrodes, and the output characteristics were measured under illumination (Figure S1) to ensure functionality. A higher drain current was observed when the transistor was illuminated than in the dark at any applied gate bias. The incident optical power was obtained in situ using a laser power meter placed above the transistor base allowing us to obtain the average incident power without disturbing the transistor configuration.

2.2. Illumination Power Dependence. When the incident power on the transistor was varied, the transfer curves given in Figure 1b were obtained. The evolution of the photocurrent, which is the difference between the drain current in the dark and illuminated measurements, as a function of the gate voltage for different illumination powers is shown in Figure S2.

A dark measurement was made between each pair of illuminated measurements for consistency and to confirm that the transistor had been restored to its default electrical setting. The difference between the dark drain current, I_D, and the illuminated drain current, I_D^{λ}, is denoted as the photocurrent, ΔI_D. Under irradiation, the drain current increased in both the *on* and *off* states. For example, the drain current more than doubles from −3.48 to −8.30 μA (ΔI_D = 4.8 μA) when the device is illuminated at a power of 29 μW with V_{GS} = V_{DS} = −40 V.

https://doi.org/10.1021/acsaelm.2c00970
ACS Appl. Electron. Mater. 2022, 4, 5799−5808

The transfer characteristics curve also shifted to more positive voltage values when light was applied. The hole mobility in the saturation regime at incident illumination powers ranging from 1.38 to 59.4 μW was 0.03 ± 0.01 cm^2/(V s) and was comparable to the corresponding hole mobility in the dark. The linear mobility also stayed constant at 0.02 ± 0.01 cm^2/(V s) during illumination. The subthreshold swing increased with the illumination power, which shows that the transistor is slower in switching from the off to the on state under illumination than in the dark. The drain current increased as a function of illumination power and the highest drain current resulted from the maximum illumination power. The difference, ΔI_D, between the drain current in the dark and under illumination increases monotonically with increasing incident power as illustrated in Figure 2a, but the increase slows down at higher illumination power.

2.3. Photovoltaic/Photoconductive Effects. Depending on the state of operation of an organic transistor during photoillumination, two effects are possible: the photovoltaic effect is observed when the transistor is operating in the on-state ($V_{GS} > V_T$), and the photoconductive effect is seen when the device is off ($V_{GS} < V_T$).

2.3.1. Photovoltaic Effects. The photocurrent as a function of the incident power has been studied in the past for both organic and inorganic semiconductors.[18−21] When a transistor is illuminated and a bias is applied, the photovoltage induced by the holes in the active layer gives rise to a significant increase in current. The photovoltaic effect is responsible for this observation and was first used to explain the optical gain of phototransistors.[22,23] For a fixed V_{GS}, the drain current changes by ΔI_D as a result of illumination, and the continuity equation relates the electron current and the electron flux at the source leading to

$$\frac{P\eta_{ext}^{\lambda}\lambda}{hc} + \frac{I_{pd}}{q} = \frac{\Delta n}{\tau_{eff}} \tag{1}$$

where η_{ext}^{λ} is the external quantum efficiency, P is the incident optical power, I_{pd} is the dark current for electrons, τ_{eff} is the shortest lifetime of trapping/recombination/diffusion, and λ is the wavelength of the illumination. The external quantum efficiency gives the ratio of the number of charges measured to the number of *incident* photons, in contrast to the internal quantum efficiency, which gives the ratio of the number of charges measured to the number of *absorbed* photons. Δn is the number of electrons accumulated at the potential minimum, which follows Boltzmann statistics.[24]

Simplifying

$$\Delta I_D = \frac{BG_m k_B T}{q} \ln\left(1 + \frac{\eta_{ext}^{\lambda}\lambda q P}{I_{pd} hc}\right) \tag{2}$$

and plotting ΔI_D as a function of P, the value of the unknown term $\frac{\eta_{ext}^{\lambda}}{I_{pd}}$ can be obtained. Here, G_m is the transconductance, T is the temperature, and k_B is the Boltzmann's constant. The parameter B was calculated to be 241, and $\frac{\eta_{ext}^{\lambda}}{I_{pd}}$ of 0.89 μA^{-1} was obtained; the fit can be seen in Figure 2a in orange color. The excellent correlation between the data points and the best-fit curve shows that the transistor is governed by the photovoltaic effect in the saturation regime and eq 2 can be used to accurately model the dependence of the photocurrent on the incident power. In addition, with a single illumination measurement (along with $\Delta I_D = 0$ when $P = 0$), the magnitude of the photocurrent can be accurately determined for other illumination powers, which is useful when designing and optimizing photodetectors. The external quantum efficiency, η_{ext}^{λ}, of the transistor cannot be calculated because the electronic dark current, I_{pd}, is unknown and our attempts to measure the dark current due to electrons for this material have not been successful. When one assumes that the external quantum efficiency cannot be larger than 100%, an upper bound for I_{pd} is obtained to be 1.13 μA. The very high dark current suggests that either the model is not robust or η_{ext}^{λ} is *higher* than 100%. We have shown previously that η_{ext}^{λ} is indeed larger than 100% for diF-TES ADT OFETs when gold is used as the contact material.[25] By comparing the number of photons absorbed to the number of charges generated in the material, we counted more charges collected at the drain terminal during channel illumination and attributed this increase to lowering of the potential barrier between the organic semiconductor and the gold electrode due to accumulation of photogenerated electrons in the organic layer.

For very low illumination powers (nW or smaller), the above equation can simplified by a Taylor expansion of the function to the first order near zero illumination power ($\ln[1 + x] \approx x$)

$$\Delta I_D = \frac{Bk_B T\eta_{ext}^{\lambda}\lambda P}{I_{pd} hc} \tag{3}$$

which would manifest as a straight line through the origin with a constant slope $\left(\frac{Bk_B T\eta_{ext}^{\lambda}\lambda}{I_{pd} hc}\right)$ of the ΔI_D−P graph.

2.3.2. Photoconductive Effects. The photoconductive effect arises from the generation of mobile carriers from illumination throughout the bulk semiconductor between source and drain, the number of which increases with the photon flux. The photocurrents as a function of the light intensity in the on and off states were modeled accurately by the equations below.[26] The photoconductive effect occurs when the device is operating in the saturation regime but in the turned-off state ($V_{GS} > V_T$). In this state, photogenerated holes increase the channel conductivity, and the drain current is described by[27,28]

$$I_D = pA_d vq = p\mu qEA_d\Delta I_D = \Delta p\mu q\frac{V_{DS}}{L}Wt_s \tag{4}$$

where $A_d = Wt$ is the cross-sectional area of the film, v is the drift velocity, p (Δp) is the (photoinduced) carrier density, E is the electric field in the channel (which can be approximated as $\frac{V_{DS}}{L}$), and t_s is the thickness of the semiconductor, which is used to evaluate the drift velocity of charge carriers in semiconductors. Noh et al. demonstrated that ΔI_D varies linearly with the power[26], which leads to

$$\Delta I_D = \Delta p\mu q\frac{V_{DS}}{L}Wt_s = CP \tag{5}$$

with C being a fitting constant. By finding the functional relationship between ΔI_D and P, the increase in the hole density due to photoexcitation can be evaluated. The plot is shown in Figure 2b. From the plot of $|\Delta I_D|$ vs P, the fitting parameter C is determined to be 0.0045 V^{-1}, and using μ_{sat} = 0.03 cm^2/(V s), L = 50 μm, t_s = 67 nm, and W = 800 μm, we calculated the photoinduced hole concentration in the channel to be

$$\frac{\Delta p}{P} = \frac{C}{\mu q\frac{V_{DS}}{L}Wt} = 2.2 \times 10^{20}\ \text{cm}^{-3}\text{W}^{-1} \tag{6}$$

The photoinduced carrier concentration per unit power, $\Delta p/P$, obtained is 2.2 × 10^{20} cm^{-3}W^{-1}, which is an approximation of the photoinduced carrier density in the channel as an effect of illumination. Comparing this number to the total hole concentration that is theoretically possible if *each* incident photon generates a conducting hole with 100% conversion efficiency, we obtain

$$\frac{p_{hole}}{P} = \frac{1}{E} = \frac{\lambda}{hc} = 2.7 \times 10^{18}\ \text{cm}^{-3}\text{W}^{-1}. \tag{7}$$

When one assumes that the number of carriers in the bulk of the material is equal to the carrier density in the transistor channel, the calculated value of p_{hole} (2.7 × 10^{18} cm^{-3}) is 2 orders of magnitude smaller than Δp, which again reinforces the fact that the efficiency is higher than 100% in our transistors.

Comparable results were obtained by repeating the measurements with different transistors that had similar contact resistance and channel dimensions in the same configuration. Patterning the semiconductor using a metallic scribe to isolate each transistor from its neighbors prevents charges from adjacent devices from "leaking" into the device during operation. The nonscribed transistors had

https://doi.org/10.1021/acsaelm.2c00970
ACS Appl. Electron. Mater. 2022, 4, 5799−5808

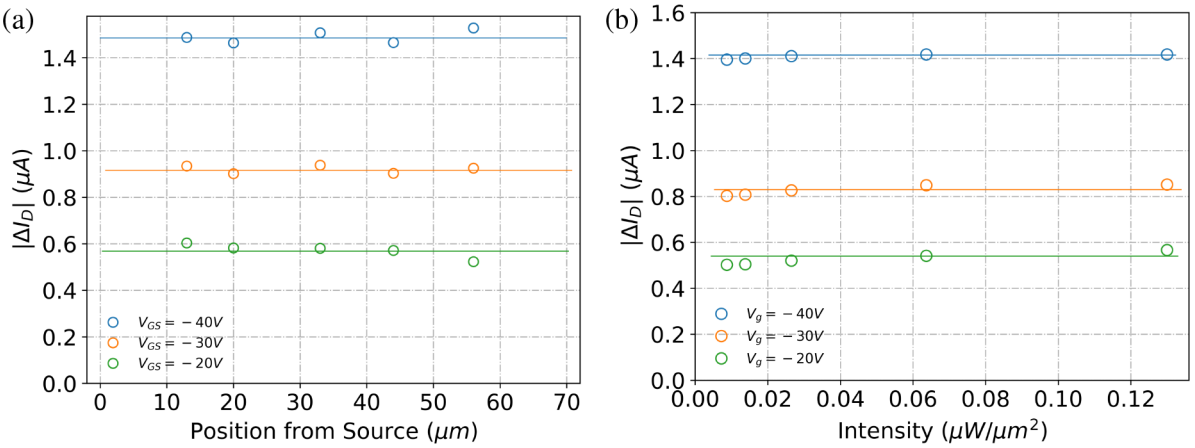

Figure 3. (a) Photocurrent at multiple channel positions from the source. (b) Photocurrent as a function of the illumination intensity by changing the spot size of the laser source.

lower overall performance due to higher leakage, but all the plots had similar trends.

2.4. Spot and Position Dependence. We investigated the effect of the location of the laser spot in the channel by moving the illumination spot across the channel from the source to the drain and the effect of the spot diameter by focusing and defocusing the laser spot.

Current−voltage measurements were taken during illumination of different sections of the channel of the transistor by keeping the focal distance fixed. Due to heavy scattering from the laser beam, the laser spot position had to be estimated by assuming a symmetrical Gaussian beam. To maximize the number of measurements before reaching the edge of the electrode, we opted for a transistor with a larger channel (70 μm). Device characteristics were measured with the laser spot at 5 distinct positions in the channel when the transistor was operating under the saturation regime; the laser spot was kept halfway between the top and bottom of the channel. Using the razor blade method, the size of the laser spot was measured to be approximately 9 μm for green light. A plot of the photocurrent as a function of the position of the laser spot relative to the source is given in Figure 3a. We observed that, for any gate voltage, the photocurrent did not change regardless of the location of the laser spot in the channel. A horizontal line in the figure shows the constancy of the photocurrent at multiple gate−source voltage measurements (V_{GS} = −40, −30, −20 V). Other device parameters also did not change, which suggests that the location of the laser spot in the channel is not critical as long as the number of photons incident in the channel of the transistor is the same. Other organic thin-film transistors have been shown to generate higher photocurrent when light is closer to the drain/source.[29]

As the laser power was kept constant in all cases, the same number of free carriers is generated at each location. The uniformity of our results means that the mean free path of the carrier before getting trapped is smaller than approximately 15 μm based on Figure 3a, which agrees with what has been reported in the literature.[30]

We devised a follow-up experiment in which the laser spot size on the channel of the transistor was increased by moving the transistor farther from the objective and defocusing the laser spot. The illumination intensity (power per unit area) was thus varied for the same total power. The photocurrent during saturation (V_{DS} = −40 V) at multiple gate−source voltages (V_{GS} = −20, −30, and −40 V) is plotted in Figure 3b as a function of the illumination intensity. Similar results were obtained as when the illumination position was varied; the carrier mobility, threshold voltage, and the subthreshold swing remained unchanged regardless of the laser *intensity* on the active layer. Having a high density of excitons in a localized region does not impact any properties of the transistor and is equivalent to having a low density of carriers in a larger region. The total number of carriers generated in the semiconductor is the same in both cases.

The constancy of the photocurrent, carrier mobility, threshold voltage, and subthreshold slope when an equal number of photons are absorbed by the semiconductor layer is pertinent for light-detection applications because the same response is desired from a phototransistor regardless of where the light is falling on the channel of the transistor. Our results suggest that the response of a photodetector based on diF-TES ADT will be homogeneous as long as the film morphology is uniform.

3. METRICS OF PHOTODETECTORS

In this section, the figures of merit that are used to quantify the optical response of the diF-TES ADT photodetector will be discussed.

3.1. Photosensitivity. The photosensitivity, S, corresponds to the signal-to-noise ratio (photocurrent to dark current) of the detector. It is a unitless parameter and is expressed as

$$S = \left.\frac{I_D^{\lambda} - I_D}{I_D}\right|_{V_{GS}} = \left.\frac{\Delta I_D}{I_D}\right|_{V_{GS}} \tag{8}$$

where I_D^{λ} and I_D are the drain currents measured at the same gate−source voltage under illumination and in the dark, respectively. S was calculated from the transfer characteristics of the diF-TES ADT transistor in both the linear regime and saturation regime using a wavelength of 532 nm as a function of V_{GS} (see Figure S3).

The maximum photosensitivity for an illumination power of 29 μW was 133 at V_{GS} = −2 V, which occurred when the transistor was off (V_T = −8.1 V). The photosensitivity plummeted as V_{GS} was swept to more negative values and was at its lowest value (S = 2.0) when the transistor was fully on (V_{DS} = V_{GS} = −40 V). The decrease in the photosensitivity values shows that the photovoltaic effect overtakes the photoconductive effect as the transistor turns on. The photoconductive effect is dominant when the transistor is off as the hole population is amplified by photogenerated charges (photoconduction), which increases the off-current. In the photovoltaic mode, this effect is no longer prominent as holes are also being injected from the source terminal both in the dark and during illumination (strong accumulation). As such, the maximum sensitivity demarcates the transition between photoconductive and photovoltaic effects. As expected, the maximum photosensitivity was much lower in the linear

https://doi.org/10.1021/acsaelm.2c00970
ACS Appl. Electron. Mater. 2022, 4, 5799−5808

regime: $S \approx 11$ at $V_{GS} = -2$ V. The side-by-side comparison in the linear and saturation regimes of S is included in Figure S3.

Using the transfer characteristics, the photosensitivity was also calculated at different illumination powers, and the maximum sensitivity is plotted as a function of the incident power in Figure 4 for the saturation regime and in Figure S4 for the linear regime.

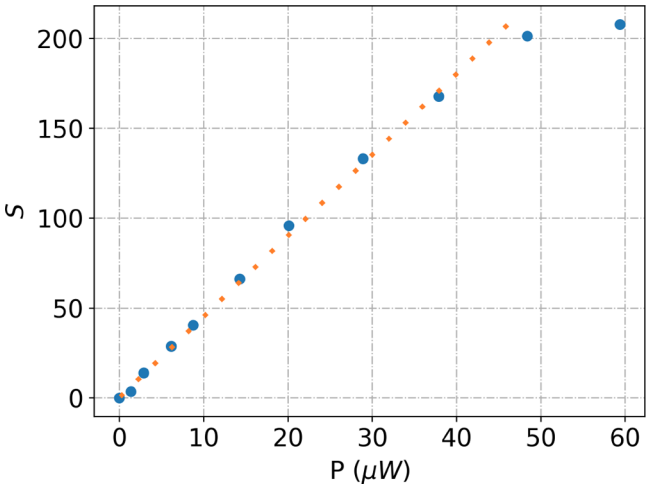

Figure 4. Maximum photosensitivity in the saturation regime using a 532 nm wavelength and average dark current as a function of incident illumination power with the fitted line.

Narayan and Kumar showed that there is a direct correlation between the photosensitivity, the flux rate, and the thickness of the semiconductor.[21] At low incident illumination power, the sensitivity increases linearly (Figure 4) and starts to deviate from linear behavior above 20 μW in both regimes. The deviation is possibly because the photovoltaic effect starts to saturate. A similar behavior was seen for the photocurrent in Figure 2a caused by saturation of trapped electrons at the interface. The maximum photosensitivity of 208 was obtained at the highest illumination power of 59 μW, which compares well with that of other organic phototransistors ($S \sim 100$)[31,32] consisting of a single organic material.

A similar metric to the photosensitivity is the current gain, $R_{D/L}$ (or photoresponse), which is the ratio of the drain current during illumination to the drain current in the dark of a photodetector at a specific gate−source voltage[33]

$$R_{D/L} = \left.\frac{I_D^{\lambda}}{I_D}\right|_{V_{GS}} \tag{9}$$

The current gain (Figure S5) and the photosensitivity (Figure 4) are very similar since the drain current during illumination overpowers the drain current in the dark during device saturation.

3.2. Photoresponsivity. Although the photosensitivity is useful as a comparative tool, it is heavily dependent on the incident power, and we have already shown that higher illumination favors higher photosensitivity values. The photoresponsivity normalizes this value to the incident power and gives the yield of a photodetector, that is the increase in the measured current per unit optical power. The photoresponsivity, R, is given by

$$R = \frac{I_D^{\lambda} - I_D}{P_u A_d} = \frac{\Delta I_D}{P_u A} = \frac{\Delta I_D}{P} \tag{10}$$

where P_u is the power per unit area of the incident light and A_d is the effective device area. A_d is calculated from the geometry of the device and equals the product of the length (L) and width (W) of the channel for full channel illumination. In our case, P is the incident power that we are using as the spot size is smaller than the channel and all of the illumination falls in the channel. The photoresponsivity is highest when the device is operating in the strong accumulation mode because the photocurrent is highest in the saturation regime as seen from the plot of photoresponsivity, R, versus the gate−source voltage, V_{GS} (Figure 5b).

The photoresponsivity generally decreases with increasing illumination power for both organic and inorganic phototransistors,[34,35] but there are also reports which show that R increases with illumination power.[36,37] On the basis of the limited body of research available, the exact cause is not known; however, it seems that the device contact plays an important factor in this type of behavior. We computed the photoresponsivity at different illumination powers, and the result is presented in Figure 6b. When one focuses on the green wavelength from that figure, the photoresponsivity of the diF-TES ADT transistor is higher at low incident powers and decreases quickly with increasing illumination. The maximum photoresponsivity that we measured when $V_{DS} = V_{GS} = -40$ V was 730 mA/W at 532 nm. The value of the photoresponsivity is high because the semiconductor strongly absorbs green light

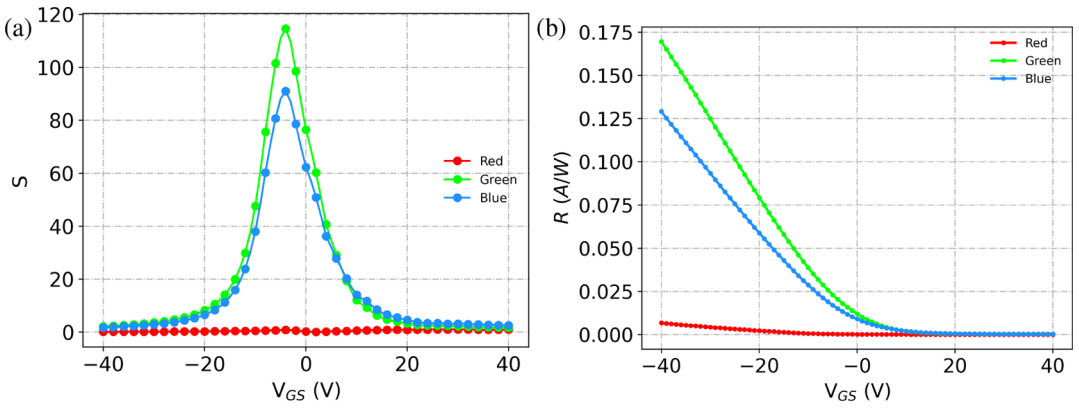

Figure 5. (a) Photosensitivity and (b) photoresponsivity of a diF-TES ADT OFET as a function of the gate voltage in the saturation regime (at $V_{DS} = -40$ V) at a power of ~37 μW using red, blue, and green wavelengths.

https://doi.org/10.1021/acsaelm.2c00970
ACS Appl. Electron. Mater. 2022, 4, 5799−5808

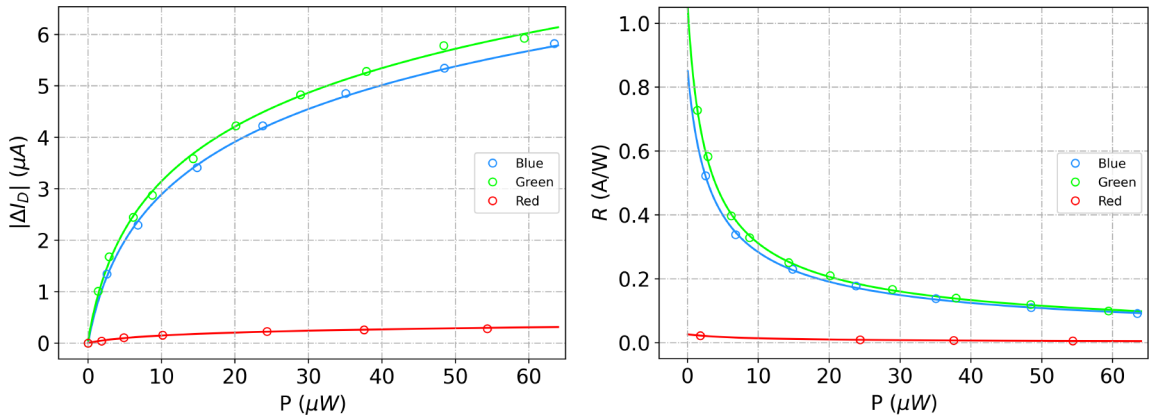

Figure 6. (a) Functions showing the behavior of red, blue, and green photocurrent at higher powers using eq 3 and (b) photoresponsivity for 633 nm (red), 532 nm (green), and 473 nm (blue) vs incident power at $V_{GS} = V_{DS} = -40$ V.

(532 nm). To our knowledge, this is one of the highest photoresponsivities in the visible spectrum based on organic semiconductors or hybrid materials and only a handful of OFETs have photoresponsivities larger than 200 mA/W.[12]

We have demonstrated in the previous section that the photocurrent has a logarithmic dependence on the illumination power ($\Delta I_D = a \ln[1 + bP]$), so R can be extrapolated using

$$R = \frac{\Delta I_D}{P} = \frac{1.373 \ln(1 + 0.767P)}{P} \tag{11}$$

We used this functional form to fit the photoresponsivity as illustrated in Figure 6b to get the maximum theoretical photoresponsivity as the power approaches zero. We simplified using l'Hopital's rule ($R = 0/0$ as $P \to 0$)

$$R_{P\to 0} = \lim_{P\to 0} 1.373 \frac{\ln(1 + 0.767P)}{P} = 1.373 \lim_{P\to 0} \frac{\frac{d}{dP}\ln(1 + 0.767P)}{\frac{d}{dP}P} = 1053 \text{ mA/W} \tag{12}$$

The value of 1053 mA/W is the maximum theoretical photoresponsivity as the incident power approaches zero. At large values of P, the photoresponsivity can be approximated as a Puiseux series

$$R = 1.373 \frac{\ln(P) - 0.364214}{P} \tag{13}$$

which approaches zero for very high illumination intensities.

An alternative definition of the photoresponsivity is[38]

$$R = \eta_{ext}^{\lambda} \frac{q}{E} \tag{14}$$

where η_{ext}^{λ} is the external efficiency of the photodetector and gives the efficiency at which an optical signal is converted into an electrical signal. E ($=hc/\lambda$) is the energy of the incident photon in units of eV, and E for a 532 nm wavelength is 2.33 eV. Solving for

$$\eta_{ext}^{\lambda} = \frac{ER}{q} = \frac{hcR}{\lambda q} = E(eV)R \tag{15}$$

we calculated η_{ext}^{λ} to be 1.67 (or 167%) at $P = 1.38$ μW, which is possible due to photoassisted charge injection as explained in our earlier work.[25] The number of photoinduced carriers that was measured is higher than the maximum theoretical number of carriers that is generated by illumination if each photon creates an exciton. Holes from exciton generation either recombine or increase the number of mobile carriers in the conducting channel, which contribute to the drain current. On the other hand, photogenerated electrons accumulate at the interface or the source terminal, which lower the potential barrier and assist in charge injection. The amplification of the photocurrent by illumination leads to external quantum efficiencies larger than 100%. η_{ext}^{λ} decreases to 0.21 at $P = 59$ μW due to the charge saturation at higher illumination powers. The theoretical maximum value of η_{ext}^{λ} that can be achieved with this particular transistor is 2.45, which is much higher than what is reported elsewhere ($\eta_{ext}^{\lambda} \sim 0.4$ calculated from the reported values of R at 532 nm[39,40]). We will also compare, in the next section, the external quantum efficiency of a diF-TES ADT transistor to that of commercially available silicon photodetectors.

In this section, we have shown that the (maximum) photosensitivity separates the photovoltaic and photoconductive regimes. S was highest when the transistor was off in the saturation regime. The photosensitivity depended on the incident illumination power, and at the highest optical power available to us, we obtained a photosensitivity of 208. On the other hand, the photoresponsivity was highest at low illumination powers and decreased with increasing power. The maximum photoresponsivity that we obtained experimentally using 532 nm incident light was 730 mA/W at the lowest incident power and could increase up to a theoretical value of 1053 mA/W. The photoresponsivity decreased systematically with increasing illumination power, and our model predicts that the latter approaches zero at very large illumination powers, which suggests that phototransistors based on diF-TES ADT are better suited for use in low light detection applications. The external quantum efficiency using 532 nm was found to be higher than 100% due to charge injection assisted by photons.

4. WAVELENGTH DEPENDENCE OF PHOTOCURRENT

We also investigated the wavelength dependence of the photocurrent using three different monochromatic sources by illuminating the diF-TES ADT OFET with roughly the same incident power, P (633 nm) = 37.6 μW, P (532 nm) = 37.9 μW, and P (473 nm) = 35.1 μW, and measuring the transfer characteristics. Using these results, the transistor metrics were calculated and the highest photoresponse was obtained with

https://doi.org/10.1021/acsaelm.2c00970
ACS Appl. Electron. Mater. 2022, 4, 5799−5808

Table 1. Photodetector Metrics for Red, Green, and Blue Lights

Color	A	E (eV)	$\lvert\Delta I_D\rvert$ (μA)	S ($P \approx 36$ μW)	$R(A/W)$ ($P \approx 1.5$ μW)	$R(A/W)$ ($P \approx 36$ μW)	$R(A/W)$ ($P \to 0$)	η^{λ}_{ext} ($P \to 0$)	S/A	R_{max}/A
Red	0.00115	1.96	0.26	3.02	0.022	0.007	0.0266	0.0521	2630	23.1
Green	0.0420	2.33	5.28	115	0.73	0.139	1.05	2.45	2740	25.0
Blue	0.0378	2.62	4.86	91.3	0.57	0.138	0.850	2.23	2420	22.5

green light followed by blue, while red light produced the lowest response. The photocurrent clearly shows that there is a direct correlation between the photoresponse and the absorbance of diF-TES ADT (refer to Figure 8). The photocurrent is given in Table 1, and it scales with the absorbance (A) of the organic material, which is the ratio of the intensity of light on the thin film to the light transmitted by it.

Table 1 shows that the drain current and thus the photocurrent was at a maximum with green light and slightly lower with blue light; very little photocurrent was observed with red light at an equivalent incident power. We also calculated the photosensitivity $\left(S = \frac{I_D^{\lambda} - I_D}{I_D}\right)$ at the same incident power for the three incident illumination colors, and the output is presented in Figure 5a as a function of gate−source voltage. Similar correspondence between the photosensitivity and the absorption of the semiconductor is observed; the highest photosensitivity was obtained when green photons were incident on the transistor. Moreover, the highest photosensitivity was obtained at the same gate−source voltage regardless of the illumination wavelength used, which suggests that the amount of energy that is absorbed by the organic semiconductor is much more important than the energy of the individual photons. We also calculated R and η^{λ}_{ext}. The high values of S, R, and η^{λ}_{ext} with multiple wavelengths show that diF-TES ADT can be used to create high efficiency photodetectors for green and blue light. The results clearly show that diF-TES ADT has a symbatic behavior as the photocurrent closely follows the absorption data. In Figure 6a, we plotted the photocurrent as a function of the incident power at a gate/drain-source voltage of −40 V from measurements made over a period of three consecutive days, which represent a slice from each of the 50 measured transfer characteristic curves.

As the incident power increased, the photocurrent increased for all wavelengths with green showing the highest photoresponse. To be able to compare the photocurrent accurately at any power, we used the photovoltaic model that was presented earlier. We fitted the photovoltaic logarithmic function to the data points for each wavelength with excellent correlation between the functional fit and the empirical data (Figure 6a). The model helps to visualize how the photocurrent at each wavelength behaves at higher power and was used to calculate the photoresponsivity (Figure 6b) and subsequently external quantum efficiency of the phototransistor at different wavelengths.

We calculated the maximum photoresponsivity of the transistor as the power is theoretically reduced to zero ($P \to 0$) as we have done previously. The results are tabulated in Table 1. The absorbance (ratio of incident light to transmitted light) of diF-TES ADT is denoted as A, and S/R is the maximum photosensitivity/responsivity in the saturation regime.

Using the photon energy (E) listed in Table 1 for the three wavelengths, we calculated the external quantum efficiency (η^{λ}_{ext}) from R. As before, we notice the same trend between η^{λ}_{ext} and A of the semiconducting material. The trend is made more apparent if we calculate R/A and S/A (normalizing to the absorption of the material). Both ratios are roughly constant for all three wavelengths, reinforcing the fact that the photoresponsivity and photosensitivity are symbatic with the absorption spectrum of the semiconductor. The behavior of ΔI_D, S, R, and η^{λ}_{ext} can thus be inferred for a diF-TES ADT based photodetector at any wavelength. Using the ratio of the corresponding quantity with the absorbance, we evaluated the photosensing parameters ΔI_D, S, R, and η^{λ}_{ext} in the visible spectrum (Figures 7 and S7) assuming that the proportionality relationship with the absorbance is maintained outside the measurement window as the illumination power approaches zero.

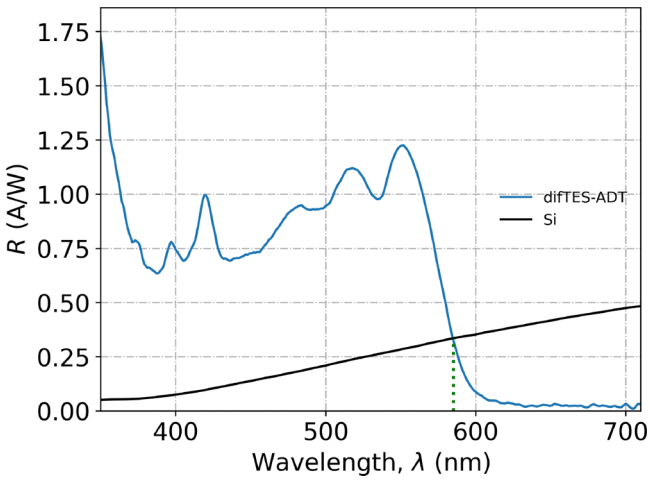

Figure 7. Blue curve: Maximum photoresponsivity as a function of illumination wavelength using data from 633, 532, and 473 nm and their absorbance. Black curve: Photoresponsivity for a commercially available silicon photodiode was digitized from the manufacturer's datasheet.[41]

DiF-TES ADT has its highest absorption band at 550 nm in the visible range, and we predict that the photoresponsivity will be approximately 1220 mA/W and the external quantum efficiency will have a maximum value of 289% $\left(\frac{\eta^{\lambda}_{ext}}{A} = 56.0\right)$ at very low illumination power. The photocurrent (ΔI_D) and photosensitivity (S) can also be calculated using the relationships given earlier.

We have shown in this section that photodetection parameters like photocurrent (ΔI_D), photosensitivity (S), photoresponsivity (R), and external quantum efficiency (η^{λ}_{ext}) are proportional to the absorption spectrum in diF-ADT TES transistors under illumination. We tested this for wavelengths across the visible spectrum and found that the ratio of the

https://doi.org/10.1021/acsaelm.2c00970
ACS Appl. Electron. Mater. 2022, 4, 5799−5808

parameters to the absorbance is the same in all three cases. The photoresponsivity and external quantum efficiency are very high for blue and green wavelengths for diF-TES ADT OFETs. Very few organic photodetectors achieve photoresponsivities above 200 mA/W, and we showed that a diF-TES ADT OFET has consistent responsivity values higher than 500 mA/W for the majority of wavelengths in the visible spectrum (λ < 575 nm). Our results show that diF-TES ADT OFET is a strong candidate for photosensing applications.

4.1. Potential Device Designs. In this section, we will propose a new transistor design that employs two organic semiconductors complementing each other in their absorption in the visible range and show that this phototransistor can exceed the performance of commercial silicon photodetectors for light detection in the electromagnetic spectrum. The external quantum efficiencies of a commercial silicon photodetector (OSI Optoelectronics[41]) with red (633 nm), blue (473 nm), and green (532 nm) wavelengths are 0.775, 0.452, and 0.609 respectively (black curve in Figure 7). The value that we obtained for η^{λ}_{ext} for red light (633 nm) pales in comparison to that of the silicon device, but the external quantum efficiency for blue and green wavelengths far exceeds that of silicon. Inherently, silicon is less efficient in the visible spectrum because it favors infrared radiation as its bandgap is 1.1 eV (bandgap of diF-TES ADT is 2.3 eV).[11] We propose a hybrid device consisting of two adjacent layers (which can be achieved by photoresist or thermal evaporation by covering half of the channel or offsetting the photomask by $W/2$) in which the second layer is composed of another organic semiconductor that absorbs red light strongly and does not dissolve diF-TES ADT (insoluble). The criterion is that the second deposited layer does not dissolve the first layer.

We exemplify this design using pentacene, which is a very common organic semiconductor. The photoresponsivity of pentacene phototransistors can reach up to 1000 mA/W at 650 nm, which would be equivalent to an external quantum efficiency of 1.91.[36] The hybrid device (diF-TES ADT + pentacene shown in the inset of Figure 8) would be an excellent photodetector for the full range of the visible electromagnetic spectrum. Since pentacene is insoluble in common organic solvents after it is deposited by thermal evaporation, diF-TES ADT can be spin-coated without the risk of removing the existing pentacene layer. The diF-TES ADT layer that will be formed on top of pentacene will not affect the photodetection properties at long wavelengths since diF-TES ADT does not absorb strongly for wavelengths larger than 575 nm, meaning that the thin layer of diF-TES ADT on top of pentacene will be transparent to the source of illumination. The proposed absorption of the combined films of diF-TES ADT and pentacene OFET is given in Figure 8. Data for pure pentacene were obtained from ref 42 and were normalized to the highest absorption peak of diF-TES ADT at 550 nm; broken lines represent the spectrum of the individual materials. The resulting hybrid thin-film transistor would exhibit quantum efficiencies larger than 100% across the visible spectrum from 350 to 700 nm.

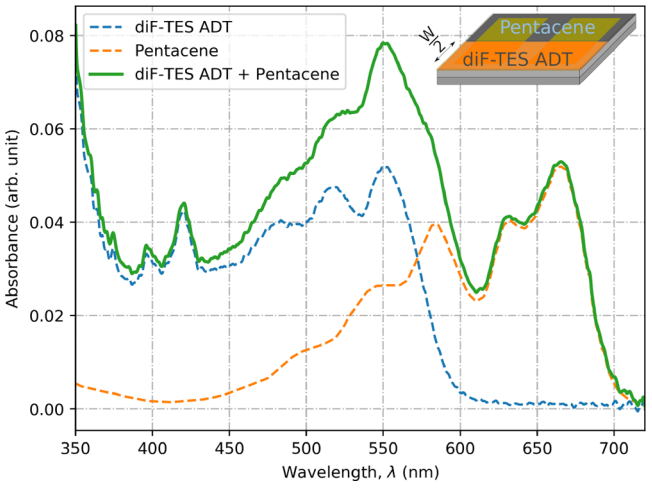

Figure 8. Absorption of a hybrid diF-TES ADT/pentacene transistor for a semiconductor thickness of 67 nm. The inset shows a hybrid pentacene and diF-TES ADT transistor.

5. CONCLUSION

In this paper, we have shown that diF-TES ADT can be a viable photosensor material. Employing a photovoltaic/photoconductive model, we were able to accurately model our experimental data. By using three separate wavelengths (red, blue, and green), our results show that the photoresponse of our transistor is proportional to the optical absorption of the organic material (symbatic response). We also achieved very high photosensitivity and photoresponsivity for green and blue light, exceeding those of other organic thin-film transistors and silicon photodetectors. Combining the results of the absorption data and the photocurrent models, we presented how a device based on diF-TES ADT would behave at any wavelengths in the visible spectrum. A similar analysis can be applied to a broad spectrum of organic semiconductors to generate their photoresponse upon illumination. We also provide a design for a hybrid device using two organic small molecules that complement one another's absorption properties; such a device would have very high optical detection performance throughout the visible spectrum. We also showed that a transistor with diF-TES ADT as the active layer is highly uniform and homogeneous; regardless of where light is incident on the channel of the transistor, the same photoresponse is measured.

■ ASSOCIATED CONTENT

Data Availability Statement

The data that support the findings of this study are available from the corresponding authors upon reasonable request.

Supporting Information

The Supporting Information is available free of charge at https://pubs.acs.org/doi/10.1021/acsaelm.2c00970.

Transistor output and transfer characteristics under illumination, photosensitivity in the linear and saturation regimes, and photodetector metrics (PDF)

■ AUTHOR INFORMATION

Corresponding Author

Zafrullah Jagoo − *Department of Physics and Astronomy, University of North Carolina at Chapel Hill, Chapel Hill, North Carolina 27599, United States;* orcid.org/0000-0001-6407-0137; Email: zaf@physicist.net

https://doi.org/10.1021/acsaelm.2c00970
ACS Appl. Electron. Mater. 2022, 4, 5799−5808

Authors

Zachary A. Lamport − *Department of Electrical Engineering, Columbia University, New York, New York 10027, United States*

Oana D. Jurchescu − *Department of Physics and Center for Functional Materials, Wake Forest University, Winston Salem, North Carolina 27109, United States;* orcid.org/0000-0003-2204-2909

Laurie E. McNeil − *Department of Physics and Astronomy, University of North Carolina at Chapel Hill, Chapel Hill, North Carolina 27599, United States;* orcid.org/0000-0001-8926-9548

Complete contact information is available at: https://pubs.acs.org/10.1021/acsaelm.2c00970

Notes

The authors declare no competing financial interest.

■ ACKNOWLEDGMENTS

The authors are indebted to Prof. J. E. Anthony for supplying diF-TES ADT. This work was supported by the National Science Foundation (NSF) under DMR-1708379. O.D.J. also acknowledges support from the NSF under award ECCS-1810273. We also wish to acknowledge the support of the Energy Frontier Research Center for absorption spectroscopy measurements.

■ REFERENCES

(1) Yoo, H.; Lee, I. S.; Jung, S.; Rho, S. M.; Kang, B. H.; Kim, H. J. A Review of Phototransistors Using Metal Oxide Semiconductors: Research Progress and Future Directions. *Adv. Mater.* **2021**, *33*, 2006091.

(2) Tavasli, A.; Gurunlu, B.; Gunturkun, D.; Isci, R.; Faraji, S. A Review on Solution-Processed Organic Phototransistors and Their Recent Developments. *Electronics* **2022**, *11*, 316.

(3) Mei, Y.; Fogel, D.; Chen, J.; Ward, J. W.; Payne, M. M.; Anthony, J. E.; Jurchescu, O. D. Interface engineering to enhance charge injection and transport in solution-deposited organic transistors. *Org. Electron.* **2017**, *50*, 100−105.

(4) Panidi, J.; Paterson, A. F.; Khim, D.; Fei, Z.; Han, Y.; Tsetseris, L.; Vourlias, G.; Patsalas, P. A.; Heeney, M.; Anthopoulos, T. D. Remarkable enhancement of the hole mobility in several organic small-molecules, polymers, and small-molecule: polymer blend transistors by simple admixing of the Lewis acid P-dopant B (C6F5) 3. *Advanced Science* **2018**, *5*, 1700290.

(5) Zeidell, A. M.; Ren, T.; Filston, D. S.; Iqbal, H. F.; Holland, E.; Bourland, J. D.; Anthony, J. E.; Jurchescu, O. D. Organic Field-Effect Transistors as Flexible, Tissue-Equivalent Radiation Dosimeters in Medical Applications. *Advanced Science* **2020**, *7*, 2001522.

(6) Mas-Torrent, M.; Durkut, M.; Hadley, P.; Ribas, X.; Rovira, C. High mobility of dithiophene-tetrathiafulvalene single-crystal organic field effect transistors. *J. Am. Chem. Soc.* **2004**, *126*, 984−985.

(7) Lamport, Z. A.; Barth, K. J.; Lee, H.; Gann, E.; Engmann, S.; Chen, H.; Guthold, M.; McCulloch, I.; Anthony, J. E.; Richter, L. J.; DeLongchamp, D. M.; Jurchescu, O. D. A simple and robust approach to reducing contact resistance in organic transistors. *Nat. Commun.* **2018**, *9*, 5130.

(8) Gershenson, M. E.; Podzorov, V.; Morpurgo, A. F. Colloquium: Electronic transport in single-crystal organic transistors. *Rev. Mod. Phys.* **2006**, *78*, 973−989.

(9) Klauk, H. Organic thin-film transistors. *Chem. Soc. Rev.* **2010**, *39*, 2643−2666.

(10) Blülle, B.; Häusermann, R.; Batlogg, B. Approaching the Trap-Free Limit in Organic Single-Crystal Field-Effect Transistors. *Phys. Rev. Applied* **2014**, *1*, 034006.

(11) Day, J.; Platt, A. D.; Ostroverkhova, O.; Subramanian, S.; Anthony, J. E. Organic semiconductor composites: Influence of additives on the transient photocurrent. *Appl. Phys. Lett.* **2009**, *94*, 013306.

(12) Baeg, K. J.; Binda, M.; Natali, D.; Caironi, M.; Noh, Y. Y. Organic light detectors: Photodiodes and phototransistors. *Adv. Mater.* **2013**, *25*, 4267−4295.

(13) Kim, J.; Cho, S.; Kim, Y. H.; Park, S. K. Highly-sensitive solution-processed 2,8-difluoro-5,11- bis(triethylsilylethynyl) anthradithiophene (diF-TESADT) phototransistors for optical sensing applications. *Org. Electron.* **2014**, *15*, 2099−2106.

(14) Tyznik, C.; Lee, J.; Sorli, J.; Liu, X.; Holland, E. K.; Day, C. S.; Anthony, J. E.; Loo, Y.-L.; Vardeny, Z. V.; Jurchescu, O. D. Photocurrent in metal-halide perovskite/organic semiconductor heterostructures: impact of microstructure on charge generation efficiency. *ACS Appl. Mater. Interfaces* **2021**, *13*, 10231−10238.

(15) Lamport, Z. A.; Haneef, H. F.; Anand, S.; Waldrip, M.; Jurchescu, O. D. Tutorial: Organic field-effect transistors: Materials, structure and operation. *J. Appl. Phys.* **2018**, *124*, 071101.

(16) Bittle, E. G.; Basham, J. I.; Jackson, T. N.; Jurchescu, O. D.; Gundlach, D. J. Mobility overestimation due to gated contacts in organic field-effect transistors. *Nat. Commun.* **2016**, *7*, 10908.

(17) Waldrip, M.; Jurchescu, O. D.; Gundlach, D. J.; Bittle, E. G. Contact Resistance in Organic Field-Effect Transistors: Conquering the Barrier. *Adv. Funct. Mater.* **2020**, *30*, 1904576.

(18) Madjar, A.; Herczfeld, P. R.; Paolella, A. Analytical model for optically generated currents in GaAs MESFETs. *IEEE transactions on microwave theory and techniques* **1992**, *40*, 1681−1691.

(19) Romero, M. A.; Martinez, M.; Herczfeld, P. R. An analytical model for the photodetection mechanisms in high-electron mobility transistors. *IEEE transactions on microwave theory and techniques* **1996**, *44*, 2279−2287.

(20) Hamilton, M. C.; Martin, S.; Kanicki, J. Thin-film organic polymer phototransistors. *IEEE Trans. Electron Devices* **2004**, *51*, 877−885.

(21) Narayan, K. S.; Kumar, N. Light responsive polymer field-effect transistor. *Appl. Phys. Lett.* **2001**, *79*, 1891−1893.

(22) Bube, R. H.*Photoconductivity of solids*; RE Krieger Pub. Co., 1978.

(23) Takanashi, Y.; Takahata, K.; Muramoto, Y. Characteristics of InAlAs/InGaAs high-electron-mobility transistors under illumination with modulated light. *IEEE Trans. Electron Devices* **1999**, *46*, 2271−2277.

(24) Chen, C. Y. Theory of a modulated barrier photodiode. *Appl. Phys. Lett.* **1981**, *39*, 979−981.

(25) Jagoo, Z.; Lamport, Z. A.; Jurchescu, O. D.; McNeil, L. E. Efficiency enhancement of organic thin-film phototransistors due to photoassisted charge injection. *Appl. Phys. Lett.* **2021**, *119*, 073302.

(26) Noh, Y. Y.; Kim, D. Y.; Yase, K. Highly sensitive thin-film organic phototransistors: Effect of wavelength of light source on device performance. *J. Appl. Phys.* **2005**, *98*, 074505.

(27) Kang, H. S.; Choi, C. S.; Choi, W. Y.; Kim, D. H.; Seo, K. S. Characterization of phototransistor internal gain in metamorphic high-electron-mobility transistors. *Appl. Phys. Lett.* **2004**, *84*, 3780−3782.

(28) Sze, S. M.; Ng, K. K.*Physics of semiconductor devices*; John Wiley & Sons, 2006.

(29) Jia, Z.; Shi, M.; Jia, I. Study of local mobility in pentacene field-effect transistors using spatially resolved photocurrent measurement. *IEEE Electron Device Lett.* **2010**, *31*, 761−763.

(30) Glaeser, R. M.; Berry, R. S. Mobilities of Electrons and Holes in Organic Molecular Solids. Comparison of Band and Hopping Models. *J. Chem. Phys.* **1966**, *44*, 3797−3810.

(31) Hamilton, M. C.; Kanicki, J. Organic polymer thin-film transistor photosensors. *IEEE Journal on Selected Topics in Quantum Electronics* **2004**, *10*, 840−848.

(32) Yakuphanoglu, F.; Farooq, W. A. Flexible pentacene organic field-effect phototransistor. *Synth. Met.* **2011**, *161*, 379−383.

(33) Gallezot, J.; Martin, S.; Kanicki, J. Photosensitivity of a-Si:H TFTs. *Proc. Int. Display Research Conf. (IDRC)* **2001**, 407−410.
(34) Choi, C. S.; Kang, H. S.; Choi, W. Y.; Kim, H. J.; Choi, W. J.; Kim, D. H.; Jang, K. C.; Seo, K. S. High optical responsivity of InAlAs-InGaAs metamorphic high-electron mobility transistor on GaAs substrate with composite channels. *IEEE Photonics Technology Letters* **2003**, *15*, 846−848.
(35) Lim, B. T.; Cho, J.; Cheon, K. H.; Shin, K.; Chung, D. S. Photoconductive behaviors of difluorinated 5,11-bis-(triethylsilylethynyl) anthradithiophene. *Org. Electron.* **2015**, *18*, 113−117.
(36) Noh, Y. Y.; Kim, D. Y. Organic phototransistor based on pentacene as an efficient red light sensor. *Solid-State Electron.* **2007**, *51*, 1052−1055.
(37) Gunduz, B.; Yakuphanoglu, F. Effects of UV and white light illuminations on photosensing properties of the 6,13-bis-(triisopropylsilylethynyl)pentacene thin film transistor. *Sensors and Actuators, A: Physical* **2012**, *178*, 141−153.
(38) Bhattacharya, P.*Semiconductor Optoelectronic Devices*; Prentice Hall, 1997.
(39) He, Y.; Quinn, J. T.; Hou, D.; Ngai, J. H.; Li, Y. A small bandgap (3E,7 E)-3,7-bis(2-oxoindolin-3-ylidene)benzo[1,2-b:4,5- b ']difuran-2,6(3 H,7 H)-dione (IBDF) based polymer semiconductor for near-infrared organic phototransistors. *Journal of Materials Chemistry C* **2017**, *5*, 12163−12171.
(40) Peng, Y.; Lv, W.; Yao, B.; Fan, G.; Chen, D.; Gao, P.; Zhou, M.; Wang, Y. High performance near infrared photosensitive organic field-effect transistors realized by an organic hybrid planar-bulk heterojunction. *Org. Electron.* **2013**, *14*, 1045−1051.
(41) OSI Optoelectronics. *Photodiode Characteristics and Applications*; http://osioptoelectronics.com/application-notes/AN-Photodiode-Parameters-Characteristics.pdf (accessed on 2022-03-12).
(42) Zhuang, J.; Lo, W. S.; Zhou, L.; Sun, Q. J.; Chan, C. F.; Zhou, Y.; Han, S. T.; Yan, Y.; Wong, W. T.; Wong, K. L.; Roy, V. A. Photoreactive charge trapping memory based on lanthanide complex. *Sci. Rep.* **2015**, *5*, 14998.

https://doi.org/10.1021/acsaelm.2c00970
ACS Appl. Electron. Mater. 2022, 4, 5799−5808